



Contents lists available at ScienceDirect

Commun Nonlinear Sci Numer Simulat

journal homepage: www.elsevier.com/locate/cnsns

Calculation of added mass coefficients of 3D complicated underwater bodies by FMBEM

Zhiliang Lin, Shijun Liao*

State Key Lab of Ocean Engineering, School of Naval Architecture, Ocean and Civil Engineering, Shanghai Jiao Tong University, Shanghai 200240, China

ARTICLE INFO

Article history:

Received 9 February 2010

Accepted 18 February 2010

Available online 21 February 2010

Keywords:

Fast multipole boundary element method

Underwater bodies

Added mass coefficients

ABSTRACT

In this paper, the fast multiple boundary element method (FMBEM) is applied to calculate the added mass coefficients of complicated three dimensional (3D) underwater bodies. First, the accuracy and efficiency of the FMBEM for 3D Laplace's equation are investigated by using some simple 3D bodies with known added mass coefficients, such as sphere and spheroids. Then, as an example, the added mass coefficients of a SUBOFF submarine are calculated by the FMBEM. It is found that the FMBEM is computationally much more efficient than the traditional BEM. Therefore, the FMBEM provides us an effective numerical method to predict added mass coefficients of complicated underwater bodies.

© 2010 Elsevier B.V. All rights reserved.

1. Introduction

In ocean engineering, the prediction of the added forces and moments for surface ships and underwater vehicles is very important. The added mass and the added moment of inertia can be viewed as the mass and the moment of inertia of the fluid moving with the body while the body is in motion of acceleration, respectively. In potential flow, if ϕ_i represents the velocity potential of the steady flow due to unit motion of a body in the i -direction then the added mass tensor is defined as:

$$m_{ji} = -\rho \int_S \phi_i \frac{\partial \phi_j}{\partial n} dS \quad i, j = 1, 2, \dots, 6 \quad (1)$$

where ρ is the fluid density, n is the outward normal to the surface, S , which represents the body surface. m_{ji} is the added mass (or moment of inertia) in the j -direction corresponding to a motion in the i -direction. The indices 1 through 3 correspond to linear motions in x , y and z directions (surge, sway and heave), and the indices 4 through 6 correspond to rotations about the x , y and z -axes (roll, pitch, and yaw), respectively. The added mass coefficients are symmetric, i.e., $m_{ij} = m_{ji}$, therefore in general there are 21 unknown added mass coefficients. If the body is symmetrical with respect to one or more axes of symmetry, this number is reduced substantially. For details, please refer to Newman [1] or Kochin et al. [2].

The boundary element method has been widely applied to obtain the added mass coefficients for underwater bodies [3,4]. In the traditional BEM, a standard linear system of equations is formed, and coefficient matrices are fully populated. That is, the traditional BEM requires $O(N^2)$ operations to obtain the coefficients and another $O(N^3)$ operations to solve the linear system using direct solvers, where N is the number of equations of the linear system. This is a serious limitation which leads to huge exhaustion of the memory of a computer and becomes an obstacle for the applications of the traditional BEM to large-scale problems.

The fast multipole method (FMM) was pioneered by Roklin [5] as a fast solution method for integral equations for 2D Laplace's equation in the mid of 1980s. And then Greengard [6] developed FMM for the pairwise force calculation in mul-

* Corresponding author.

E-mail addresses: linzhiliang@sjtu.edu.cn (Z. Lin), sjliao@sjtu.edu.cn (S. Liao).

ti-body problems with columbic potential. FMM has been nominated as one of the top 10 algorithms of the 20th century along with Fast Fourier Transform (FFT), QR algorithm, etc., in scientific computing. With the FMM and iterative solver, a new method based on the traditional BEM [7–10] was developed, which is named fast multipole boundary element method (FMBEM). Using the FMBEM, the solution time can be reduced to $O(N)$ and the memory requirement can also be reduced to $O(N)$. The basic concepts and primary procedures in the FMBEM have been described in detail by Liu and Nishimura [11].

In this paper, the basic ideas of the FMBEM for 3D Laplace's equation are described at first. Then, the uniform potential flows past a sphere or spheroid are used as simple examples to investigate the accuracy and efficiency of the FMBEM. Finally, the added mass coefficients of the DARPA SUBOFF submarine [12] are calculated by means of the FMBEM. It is found that the FMBEM is an effective numerical method to predict the added mass of underwater bodies with complex geometry.

2. FMBEM for 3D Laplace's equation

Consider the 3D Laplace's equation governing the potential problems

$$\nabla^2 \phi(\mathbf{x}) = 0 \quad \text{in } \Omega, \tag{2}$$

subject to the boundary conditions

$$\phi(\mathbf{x}) = \bar{\phi}(\mathbf{x}) \quad \text{on } \Gamma_1, \tag{3}$$

and

$$q(\mathbf{x}) = \frac{\partial \phi(\mathbf{x})}{\partial n} = \bar{q}(\mathbf{x}) \quad \text{on } \Gamma_2, \tag{4}$$

where ϕ is the potential field in domain Ω , $\Gamma = \Gamma_1 \cup \Gamma_2$ the boundary of Ω , n is the outward normal to Γ , and the barred quantities indicate given values on the boundary.

Using the traditional BEM, one can write the solution of Laplace's equation in the form

$$\phi(\mathbf{x}) = \int_{\Gamma} \left(G(\vec{\mathbf{x}}, \vec{\mathbf{y}}) q(\mathbf{y}) - \frac{\partial G(\vec{\mathbf{x}}, \vec{\mathbf{y}})}{\partial n_y} \phi(\mathbf{y}) \right) d\Gamma(\mathbf{y}), \quad \mathbf{x} \in \Omega, \tag{5}$$

where G is the fundamental solution of the 3D Laplace's equation given by

$$G(\vec{\mathbf{x}}, \vec{\mathbf{y}}) = \frac{1}{4\pi |\vec{\mathbf{x}} - \vec{\mathbf{y}}|}, \tag{6}$$

in which $\vec{\mathbf{x}}$ is a vector from the coordinate origin o to the collocation point \mathbf{x} .

Letting $\mathbf{x} \rightarrow \Gamma$, we obtain the following boundary integral equation:

$$C(\mathbf{x})\phi(\mathbf{x}) = \int_{\Gamma} \left(G(\vec{\mathbf{x}}, \vec{\mathbf{y}}) q(\mathbf{y}) - \frac{\partial G(\vec{\mathbf{x}}, \vec{\mathbf{y}})}{\partial n_y} \phi(\mathbf{y}) \right) d\Gamma(\mathbf{y}), \quad \forall \mathbf{x} \in \Gamma; \tag{7}$$

and the coefficient

$$C(\mathbf{x}) = - \int_{\Gamma} \frac{\partial G(\vec{\mathbf{x}}, \vec{\mathbf{y}})}{\partial n_y} d\Gamma(\mathbf{y}). \tag{8}$$

If the boundary Γ is smooth at the collocation point \mathbf{x} , we have $C(\mathbf{x}) = 1/2$.

In the traditional BEM, we can use elements to subdivide the boundary and obtain a linear system $\mathbf{A}\lambda = \mathbf{b}$, where \mathbf{A} is the coefficient matrix, λ the unknown vector and \mathbf{b} the known right-hand side vector. Please refer to Brebbia's book [13] for more details about the traditional BEM.

2.1. Basic formulae

The fast multipole method is employed to accelerate the solutions of boundary integral equations. We first describe the basic formulae, such as multipole moment, moment-to-moment (M2M) translation, local expansion, moment-to-local expansion (M2L) translation and local expansion-to-local expansion (L2L) translation.

Expand the fundamental solution $G(\vec{\mathbf{x}}, \vec{\mathbf{y}})$ into a series of products of functions of \mathbf{x} and those of \mathbf{y} (Fig. 1). Note that the following expansion holds true:

$$\frac{1}{4\pi |\vec{\mathbf{x}} - \vec{\mathbf{y}}|} = \frac{1}{4\pi} \sum_{n=0}^{\infty} \sum_{m=-n}^n \overline{S_{n,m}(\mathbf{y}_c \vec{\mathbf{x}})} R_{n,m}(\mathbf{y}_c \vec{\mathbf{y}}), \quad |\mathbf{y}_c \vec{\mathbf{x}}| > |\mathbf{y}_c \vec{\mathbf{y}}|, \tag{9}$$

where $R_{n,m}$ and $S_{n,m}$ are the solid harmonics defined by

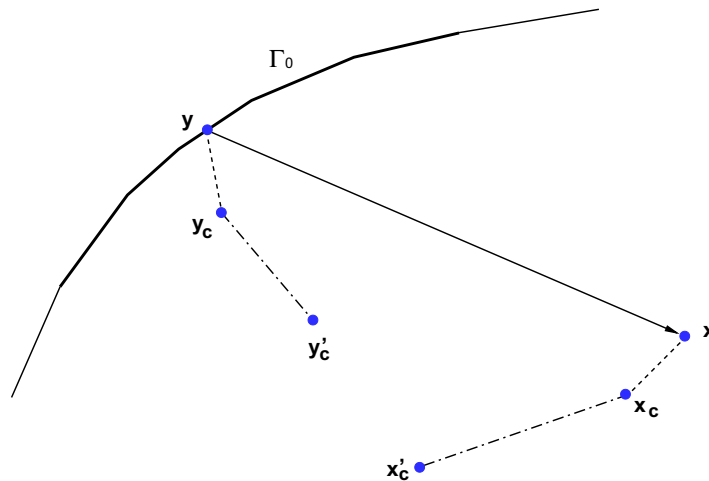


Fig. 1. Boundary and related points for fast multipole expansions.

$$R_{n,m}(\overline{\mathbf{y}_c \mathbf{x}}) = \frac{1}{(n+m)!} P_n^m(\cos\theta) e^{im\phi} r^n, \tag{10}$$

$$S_{n,m}(\overline{\mathbf{y}_c \mathbf{x}}) = (n-m)! P_n^m(\cos\theta) e^{im\phi} \frac{1}{r^{n+1}}. \tag{11}$$

(r, θ, ϕ) are the spherical coordinates of the vector $\overline{\mathbf{y}_c \mathbf{x}}$, P_n^m is the associated Legendre function and the superposed bar indicates the complex conjugate. The functions $R_{n,m}$ and $S_{n,m}$ satisfy the relations

$$R_{n,m}(\overline{\mathbf{y} \mathbf{x}}) = \sum_{n'=0}^n \sum_{m'=-n'}^{n'} R_{n',m'}(\overline{\mathbf{y} \mathbf{y}_c}) R_{n-n',m-m'}(\overline{\mathbf{y}_c \mathbf{x}}), \tag{12}$$

and

$$S_{n,m}(\overline{\mathbf{y} \mathbf{x}}) = \sum_{n'=0}^{\infty} \sum_{m'=-n'}^{n'} \overline{R_{n',m'}(\overline{\mathbf{y}_c \mathbf{y}})} S_{n+n',m+m'}(\overline{\mathbf{y}_c \mathbf{x}}), \quad |\overline{\mathbf{y}_c \mathbf{y}}| < |\overline{\mathbf{y}_c \mathbf{x}}|. \tag{13}$$

Therefore, for a part of Γ denoted by Γ_0 and a point \mathbf{x} far away from Γ_0 , the multipole expansion can be given by

$$\int_{\Gamma_0} \left(G(\overline{\mathbf{x}}, \overline{\mathbf{y}}) q(\mathbf{y}) - \frac{\partial G(\overline{\mathbf{x}}, \overline{\mathbf{y}})}{\partial n_y} \phi(\mathbf{y}) \right) d\Gamma(\mathbf{y}) = \sum_{n=0}^{\infty} \sum_{m=-n}^n \overline{S_{n,m}(\overline{\mathbf{y}_c \mathbf{x}})} M_{n,m}(\mathbf{y}_c), \tag{14}$$

where $M_{n,m}(\mathbf{y}_c)$ stands for the multipole moment centered at \mathbf{y}_c , given by

$$M_{n,m}(\mathbf{y}_c) = \int_{\Gamma_0} \left(R_{n,m}(\overline{\mathbf{y}_c \mathbf{y}}) q(\mathbf{y}) - \frac{\partial R_{n,m}(\overline{\mathbf{y}_c \mathbf{y}})}{\partial n_y} \phi(\mathbf{y}) \right) d\Gamma(\mathbf{y}). \tag{15}$$

As the origin is shifted from \mathbf{y}_c to \mathbf{y}'_c , there is the following M2M translation formula:

$$M_{n',m'}(\mathbf{y}'_c) = \sum_{n=0}^{n'} \sum_{m=-n}^n R_{n,m}(\overline{\mathbf{y}'_c \mathbf{y}_c}) M_{n'-n}^{m'-m}(\mathbf{y}_c). \tag{16}$$

The local expansion is given by

$$\int_{\Gamma_0} \left(G(\overline{\mathbf{x}}, \overline{\mathbf{y}}) q(\mathbf{y}) - \frac{\partial G(\overline{\mathbf{x}}, \overline{\mathbf{y}})}{\partial n_y} \phi(\mathbf{y}) \right) d\Gamma(\mathbf{y}) = \sum_{n=0}^{\infty} \sum_{m=-n}^n R_{n,m}(\overline{\mathbf{x}_c \mathbf{x}}) L_{n,m}(\mathbf{x}_c) \tag{17}$$

for points \mathbf{x} in the neighborhood of a certain point \mathbf{x}_c , where the coefficient of the local expansion $L_{n,m}$ is given by the following M2L translation formula:

$$L_{n,m}(\mathbf{x}_c) = \sum_{n'=0}^{\infty} \sum_{m'=-n'}^{n'} (-1)^n \overline{S_{n'+n,m'+m}(\overline{\mathbf{y}_c \mathbf{x}_c})} M_{n',m'}(\mathbf{y}_c). \tag{18}$$

The L2L translation formula takes the following form:

$$L_{n,m}(\mathbf{x}'_c) = \sum_{n'=n}^{\infty} \sum_{m'=-n'}^{n'} R_{n'-n,m'-m}(\overrightarrow{\mathbf{x}_c \mathbf{x}'_c}) L_{n',m'}(\mathbf{x}_c) \tag{19}$$

as one shifts the center of expansion from \mathbf{x}_c to \mathbf{x}'_c .

2.2. FMBEM algorithm

The main idea of the FMBEM is to translate the traditional element-to-element interactions into cell-to-cell interactions. The details of the FMBEM algorithm have been clearly described by Nishimura [15] and Liu et al. [11]. Only the main steps of the FMM algorithms for BEM are described briefly as follows:

- Step 1. Discretize the boundary S into N elements, and discretize ϕ in an ordinary manner as the traditional BEM;
- Step 2. Obtain a hierarchical tree structures of elements. For a 3D problem, first, take a cube which contains the boundary S and call it a cell of level 0. And then divide a cell (a parent cell) of level $l (l \geq 0)$ into eight sub cubes whose size is half of that of the parent cell and call any of them a cell (a child cell) of level $l + 1$ if some boundary elements belong to this sub cube. One terminates the subdivision if a cell contains less than a given number (denoted by M) of boundary elements and this childless cell is called a leaf. A oct-tree structure of cells containing all boundary elements is formed in this step;
- Step 3. Compute the moment in each cell starting from the leaves and tracing the tree structure of cells upward. In this step, Eq. (15) is used for the computation of the multipole moments and Eq. (16) for $M2M$ translations;
- Step 4. Compute the local expansion to the leaf cells starting from the level 2 cells and tracing the tree structure of cells downward. In this step, Eq. (18) is used for $M2L$ translations and Eq. (19) for $L2L$ translations;
- Step 5. Obtain two integral contributions to each element. For the evaluation of contributions with near elements, the traditional BEM is used directly. And contributions from the far elements are evaluated with the help of the local expansion, using Eq. (17);
- Step 6. Use the iterative solver GMRES to update the unknown vector in $\mathbf{A}\mathbf{z} = \mathbf{b}$, and continue at Step 3 for the matrix and unknown vector multiplication until the solution converges within a given tolerance.

2.3. A numerical example

In this paper, all the boundary surfaces are discretized into constant triangular panels. For the FMBEM, the tolerance for the iterative solver GMRES was set to 10^{-6} , the numbers of terms for both moments and local expansions to 10 and the maximum number of elements in a leaf to 100. All the computations were done on a compute node of a cluster with an Intel(R) Xeon(TM) 3.0 GHz CPU, 4.0 GB RAM. The 25 points Gaussian quadrature for triangles [14] was applied, which permits all the integrations to achieve a reasonable accuracy.

First of all, we consider a simple potential problem (Fig. 2), i.e. a flow of unit velocity past a rigid unit sphere in an unbounded domain. In this problem, the analytical solution is available. The diffraction potential ϕ_d satisfies the 3D Laplace's equation. Then solve this problem by FMBEM and the results are compared with the exact solution. The RMS error is defined as

$$E_{RMS} = \sqrt{\frac{1}{N} \sum_{i=1}^N [(\phi_d)_{exact} - (\phi_d)_{num}]^2}, \tag{20}$$

where N is the total number of the boundary elements.

As shown in Table 1 and Fig. 3, the numerical solutions converge to the exact solution as N increases. The comparison of CPU time used by FMBEM and the traditional BEM is shown in Fig. 4. The traditional BEM uses a direct solver (Gauss

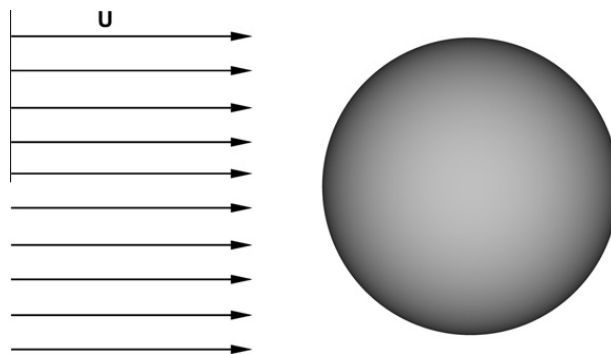


Fig. 2. Uniform flow past an unit sphere.

Table 1
RMS error versus element number.

N	184	722	1486	2896	5610	11,652	25,084	50,390	102,200
$E_{RMS} (10^{-4})$	34.17	9.32	4.79	2.42	1.24	0.61	0.28	0.14	0.07

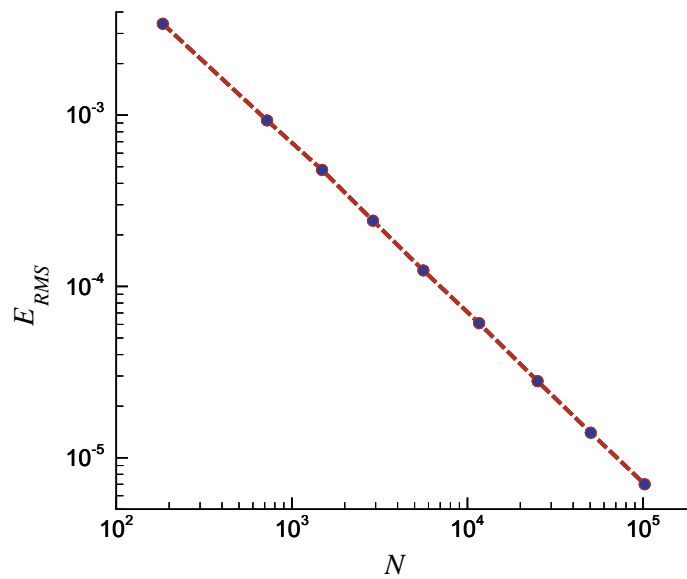


Fig. 3. RMS error versus element number.

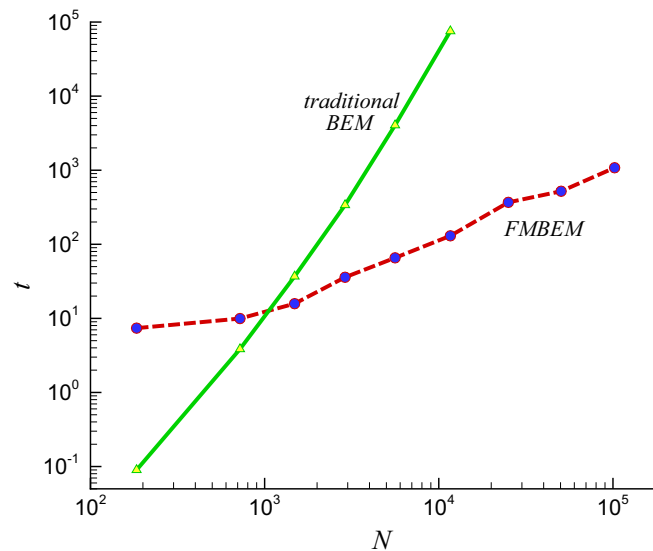


Fig. 4. Comparison of CPU time used by FMBEM and the traditional BEM.

elimination) for solving the linear system. As N , the total number of elements, is over 1000, the CPU time used by FMBEM is less than that used by the traditional BEM. As shown in Table 2, for the model with 11,652 elements, the CPU time used by FMBEM is only 130 s, while the traditional BEM used about 75,360 s. As N further increases, the memory of the computer is not enough for running the traditional BEM code, but in the case of $N = 102,200$, the CPU time used by FMBEM is less than 1080 s (18 min). As Liu et al. [11] pointed out that both the computational cost and the memory requirement can be reduced from $O(N^2)$ to $O(N)$ by FMBEM. It means that FMBEM is quite efficient and can be applied to large-scale problems.

3. Added mass calculations

In this section, the FMBEM is applied to calculate the added masses and the moments of inertia of three-dimensional bodies. First, we consider some bodies with classical shapes, such as the unit sphere and the spheroids with different

Table 2

Comparison of CPU time (s) used by FMBEM and traditional BEM.

N	184	722	1486	2896	5610	11,652	25,084	50,390	102,200
FMBEM	7.38	9.95	15.79	35.90	65.63	130.18	368.44	520.09	1079.04
BEM	0.09	3.85	36.84	338.68	4047.26	75359.57	–	–	–

slenderness ratios (a/b , where a and b are semi-axes of spheroid). At the end, the added mass coefficients of the DARPA SUB-OFF submarine are calculated.

3.1. Sphere and spheroids

For a sphere, due to the symmetry with respect to all three centroidal axes, all rotational added masses are zero, and the analytical solutions in the linear motions are: $m_{11} = m_{22} = m_{33} = 2\pi\rho a^3/3$, where a is the radius of the sphere. The non-dimensional added mass coefficients are defined as:

$$m'_{11} = m'_{22} = m'_{33} = \frac{m_{11}}{\rho a^3}. \tag{21}$$

As shown in Table 3, the added mass coefficient for the unit sphere calculated by the FMBEM agrees very well with the exact solution.

For spheroids, the rotational added masses m_{55} and m_{66} are non-zero, and there exists $m_{55} = m_{66}$. The exact solution formulas for the added masses are supplied by Sahin etc. [3]. The non-dimensional added mass coefficients are defined as:

$$\mu_x = \frac{m_{11}}{\frac{4}{3}\pi\rho ab^2}, \quad \mu_y = \mu_z = \frac{m_{22}}{\frac{4}{3}\pi\rho ab^2}, \quad \mu_{yy} = \mu_{zz} = \frac{m_{55}}{\frac{4}{15}\pi\rho ab^2(a^2 + b^2)}. \tag{22}$$

As shown in Tables 4–6, all the added mass coefficients calculated by the FMBEM converge to the exact solutions as the mesh size decreases. Here, the mesh size is the length of the equivalent sides of the triangular elements.

Thus, by refining the mesh of the boundary, we can ensure the accuracy of the FMBEM.

Table 3

Non-dimensional added mass for the unit sphere.

N	722	2896	5890	18,850	Exact solution
m'_{11}	2.0749	2.0897	2.0921	2.0937	2.0944
Relative error (%)	0.93	0.22	0.11	0.03	

Table 4

Non-dimensional added mass μ_x for spheroids with semi-axe $b = 0.5$ m.

Mesh size (m)	$a/b = 5$	$a/b = 10$	$a/b = 15$
	$\mu_x 10^2$	$\mu_x 10^2$	$\mu_x 10^2$
0.1	5.8835	2.0620	1.0818
0.05	5.9052	2.0684	1.0854
0.025	5.9105	2.0701	1.0862
Exact solution	5.9121	2.0706	1.0865

Table 5

Non-dimensional added mass μ_y for spheroids with semi-axe $b = 0.5$ m.

Mesh size (m)	$a/b = 5$	$a/b = 10$	$a/b = 15$
	μ_y	μ_y	μ_y
0.1	0.8911	0.9577	0.9764
0.05	0.8935	0.9596	0.9781
0.025	0.8941	0.9601	0.9786
Exact solution	0.8943	0.9602	0.9787

3.2. SUBOFF submarine body

The overall length of the SUBOFF submarine is 14.2917 ft. Note that the unit of length is feet, and we can compare the numerical results with the available experimental results. Two models of the SUBOFF submarines are shown in Fig. 5. One model is the bare hull and the other consists of the hull, sail configuration and stern appendages. The latter model is quite complex and the mesh strategies are shown in Figs. 6 and 7. The total number of the triangle elements is up to 27,972, but the CPU time for running the FMBEM code to obtain one added mass coefficient is only about 1660 s, less than half an hour.

Table 6

Non-dimensional added mass μ_{yy} for spheroids with semi-axis $b = 0.5$ m.

Mesh size (m)	$a/b = 5$ μ_{yy}	$a/b = 10$ μ_{yy}	$a/b = 15$ μ_{yy}
0.1	0.6951	0.8792	0.9331
0.05	0.6986	0.8824	0.9360
0.025	0.6995	0.8832	0.9368
Exact solution	0.6999	0.8835	0.9371

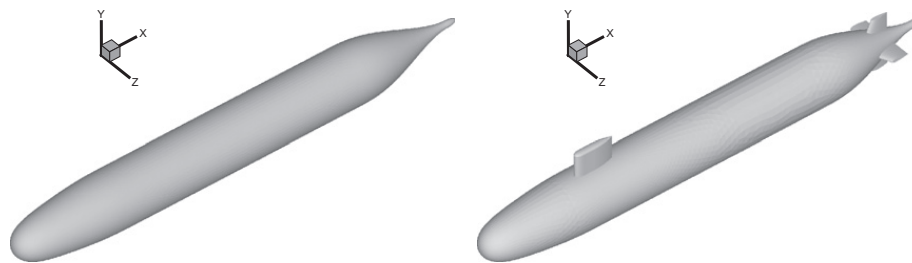


Fig. 5. The sketches of DARPA SUBOFF submarine.

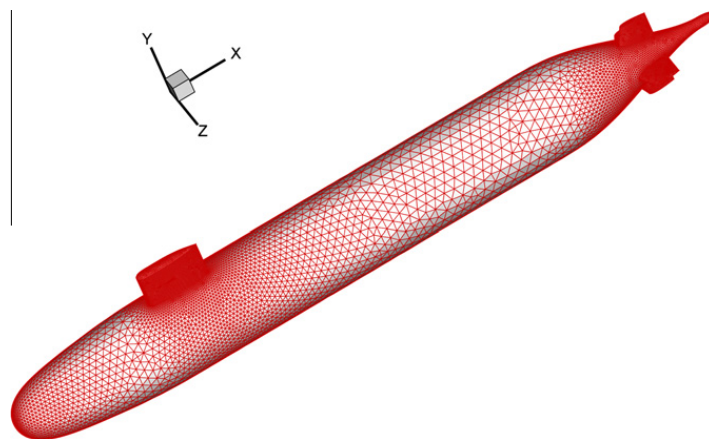


Fig. 6. The mesh of DARPA SUBOFF submarine.

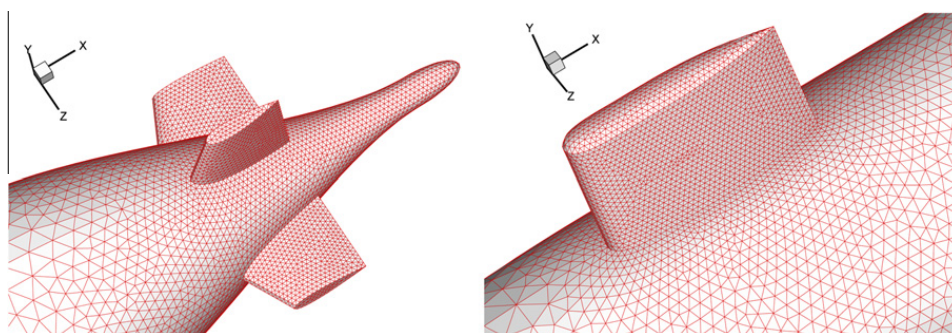


Fig. 7. The meshes of sail configuration and stern appendages.

Table 7Sway added mass (m_{22}/ρ) for the SUBOFF submarine.

N	Bare hull	Hull and sail
FMBEM	23.02	23.38
Experiment	19.40	21.95

Table 8

Added mass coefficients for the SUBOFF submarine.

	Bare hull	Hull and sail
m_{11}/ρ	0.915	0.947
m_{22}/ρ	23.023	23.376
m_{33}/ρ	23.018	24.788
m_{44}/ρ	7.7E-04	1722.750
m_{55}/ρ	1229.858	1318.279
m_{66}/ρ	1230.222	1299.018

Only the lateral motion (sway) added mass coefficients are compared with the experimental results in Table 7. The FMBEM results are close to the experimental results, which demonstrates that the results obtained by the FMBEM is reliable. Clearly, for a refine mesh, our numerical solutions will be accurate enough.

The other added masses coefficients are shown in Table 8. For the bare hull case, due to the symmetry, we have $m_{44} = 0$, $m_{22} = m_{33}$, and $m_{55} = m_{66}$. As shown in Table 8, for the bare hull, the difference between m_{22} and m_{33} is quite small, and the difference between m_{55} and m_{66} is also quite small relative to their values. Note that, the value of m_{44} equals to $7.7E-04$, which is almost zero and indicates the accuracy of the FMBEM.

Due to complex configuration of the hull and sails model, there are some interesting results. m_{33} does not equal to m_{22} , and m_{55} does not equal to m_{66} . Since the sail configuration is relatively small to the overall length, m_{33} and m_{55} are just a little greater than m_{22} and m_{66} , respectively. However, the sail configuration is in the same scale as the diameter of the SUBOFF submarine's cross section, so the existence of the sail configuration makes a great impact on the value of m_{44} . As shown in Table 8, the value of m_{44} is large rather than equal to zero.

4. Conclusions

It is costly to solve complicated 3D potential flows by means of the traditional BEM. This seriously restricts the applications of the traditional BEM to the 3D large-scale problems in ocean engineering. In this paper, the fast multipole boundary element method (FMBEM) is successfully applied to calculate the added mass coefficients of 3D underwater bodies with complicated shapes. It is found that the FMBEM is computationally much more efficient than the traditional BEM so that the number of boundary elements can be up to several millions. Thus, the FMBEM is suitable to solve 3D complicated large-scale potential problems in ocean engineering.

Acknowledgement

This work is partly supported by the National Natural Science Foundation of China (Grant Nos. 50739004 and 50509016).

References

- [1] Newman JN. Marine hydrodynamics. MIT Press; 1977.
- [2] Kochin NE, Kibel IA, Roze NV. Theoretical hydromechanics. Interscience Publishers, Wiley; 1964.
- [3] Sahin I, Crane JW, Waston KP. Added mass coefficients for submerged bodies by a low-order panel method. J Fluids Eng 1993;115:452–7.
- [4] Sahin I, Crane JW, Waston KP. Application of a panel method to hydrodynamics of underwater vehicles. Ocean Eng 1997;24(6):501–12.
- [5] Rokhlin V. Rapid solution of integral equation of classical potential theory. J Comput Phys 1985;60:187–207.
- [6] Greengard LF. The rapid evaluation of potential fields in particle systems. Cambridge: The MIT Press; 1988.
- [7] Peirce AP, Napier JAL. A spectral multipole method for efficient solution of large-scale boundary element models in elastostatics. Int J Numer Meth Eng 1995;38:4009–34.
- [8] Gomez JE, Power H. A multipole direct and indirect BEM for 2D cavity flow at low Reynolds number. Eng Anal Bound Elem 1997;19:17–31.
- [9] Nishimura N, Yoshida K, Kobayashi S. A fast multipole boundary integral equation method for crack problems in 3D. Eng Anal Bound Elem 1999;23:97–105.
- [10] Mammoli AA, Ingber MS. Stokes flow around cylinders in a bounded two-dimensional domain using multipole-accelerated boundary element methods. Int J Numer Meth Eng 1999;44:897–917.
- [11] Liu YJ, Nishimura N. The fast multipole boundary element method for potential problems: a tutorial. Eng Anal Bound Elem 2006;30:371–81.
- [12] Roddy RF. Investigation of the stability and control characteristics of several configurations of the DARPA suboff model from captive-model experiments". DTRC report SHD-1298-08; 1990.
- [13] Brebbia CA, Walker S. Boundary element techniques in engineering. London: Newnes-Butterworths; 1980.
- [14] Laursen ME, Gellert M. Some criteria for numerically integrated matrices and quadrature for formulas for triangles. Int J Numer Meth Eng 1978;12:67–76.
- [15] Nishimura N. Fast multipole accelerated boundary integral equation methods. Appl Mech Rev 2006;55(4):299–324.